Supplemental Information: High-Verdet constant and low-optical loss Tb^{3+} doped Magnetite Nanoparticles

Jan Bartos[1,‡], Taleb Ba Tis[2,‡], Mingming Nie[1], Shu-Wei Huang[1,], Wounjhang Park[1,2,*]*

[1]Department of Electrical, Computer, and Energy Engineering, University of Colorado Boulder, 80309, USA

[2] Material Science and Engineering Program, University of Colorado Boulder, 80309, USA

1. Nanoparticle synthesis and characterization

1.1 Nanoparticle synthesis Materials: iron (III) acetylacetonate (≥99.9% trace metal basis) ($Fe(acac)_3$), 1,2-hexadecanediol (technical grade, 90%) (HDD), oleic acid (technical grade, 90%) (OA), oleylamine (technical grade, 70%) (OAM), benzyl ether (98%), bis[2-(methacryloyloxy)ethyl] phosphate (BMEP), methyl methacrylate (98.5%) (MMA), azobisisobutyronitrile (98%) (AIBN) were bought from Sigma-Aldrich. Terbium acetylacetonate (99.9%) ($Tb(acac)_3$) was purchased from Fisher Scientific.

The Fe_3O_4 nanoparticle synthesis was carried out using the well-established thermal decomposition protocol with some modifications.[1,2] Briefly, 2 mmol of iron (III) acetylacetonate, $Fe(acac)_3$, was added to a three-neck round-bottom flask along with 10 mmol of 1,2-hexadecanediol (HDD), 9 mmol of oleic acid (OA), 3 mmol of oleylamine (OAM), and 20 mL of benzyl ether (BE). The temperature of flask was then raised from room temperature to 110 °C while the reagents were vigorously mixed using a magnetic stir bar. At 110 °C, the flask was kept under argon for 5 minutes followed by 5 minutes of vacuum purge. The argon/vacuum step was repeated two more times before the temperature was raised again to 180 °C under argon gas. The reaction was kept at this temperature for 2 hours before it was raised to 298 °C. Once one hour had passed at 298 °C, the reaction was allowed to cool down to room temperature.

To synthesize Tb-doped nanoparticles, some of the $Fe(acac)_3$ was replaced by terbium (III) acetylacetonate, $Tb(acac)_3$, while keeping the overall inorganic precursor content fixed at 2 mmol. For instance, 0.01 mmol of $Tb(acac)_3$ was used along with 1.99 mmol of $Fe(acac)_3$ to synthesize Fe_3O_4:Tb^{3+} (1) nanoparticles. In a similar fashion, $Tb(acac)_3$ amounts of 0.02, 0.05, 0.1, and 0.4 mmol were used to synthesize the Fe_3O_4:Tb^{3+} (2)-(5) samples, respectively. Following the synthesis, the nanoparticles were centrifuged three times using a mixture of ethanol, methanol, and acetone at 8000 RPM for 20 minutes. After that, these core nanoparticles were dispersed in a hexane solution. Larger nanoparticles were then grown using the seed-mediated growth protocol. Briefly, 80 mg of the core nanoparticles were added to the reaction flask along with (2-x) mmol $Fe(acac)_3$, (x=0.01 – 0.4) mmol $Tb(acac)_3$, 10 mmol HDD, 9 mmol OA, 3 mmol

OAM, and 20 mL BE.. All the other steps were kept the same with the slight modification of 1 hour at 180 °C and 1.5 hours at 298 °C. This seed-mediated growth step was repeated once more using the core/shell nanoparticles as seeds. Following the washing step, the final core/shell/shell nanoparticles were dispersed in chloroform and stored in a desiccator until future use.

1.2 terbium doping characterization

The exact Tb^{3+} content was confirmed via inductively coupled plasma mass spectroscopy (ICP-MS) as shown in Fig. 2 (H). The Tb^{3+} molar percentage is calculated as follows: $\mathrm{Tb(mol\%)} = \mathrm{Tb(mol)/(Fe(mol) + Tb(mol))}$. The amount of Tb^{3+} ions doped into the Fe_3O_4 nanoparticles was roughly one half the Tb^{3+} amount used in the synthesis mixture. The only exception from this trend was the Fe_3O_4: 4.55 mol% Tb^{3+} which showed only a quarter of the initial molar percentage being incorporated. This limited uptake can be, in part, due to the use of the hydrated form of the Tb^{3+} precursor, leading us to overestimate the molar amount of Tb^{3+} ions in the initial mixture. However, it is likely that the large sizes of the Tb^{3+} ions (106.3 pm) compared to the Fe^{3+} ions (78.5 pm) make it difficult to incorporate more of them without causing severe distortion to the crystal structure. Rice et al. also observed a similar limited incorporation of Tb^{3+} ions in Fe_3O_4, though to a lesser extent than what we observed.[2]

1.3 Nanoparticle characterization

The size of the nanoparticles was characterized using transmission electron microscopy (TEM) (Tecnai T12 Spirit 120kV Electron Microscope). The size distribution was calculated using the FIJI software package. The composition of the nanoparticles was confirmed by inductively-coupled plasma – mass spectroscopy (ICP-MS) (PERKIN ELMER NEXION 300Q ICP MS).

1.4 Nanoparticle surface functionalization

The native oleic-acid coating of the as-synthesized nanoparticles was replaced using the ligand exchange process with some modifications.[3] Briefly, a 10mg/mL stock solution of bis (2-methacryloxy) ethyl phosphate (BMEP) in chloroform was prepared and stored at 4 °C until use. In a separate vial, 10 mg of nanoparticles were added and dispersed in 0.7 mL chloroform via sonication. After that, 0.3 mL of the BMEP stock solution was added dropwise to the nanoparticle solution. The nanoparticle solution was then nutated overnight to complete the ligand exchange reaction. After the reaction was completed, the chloroform was dried off under vacuum, and the nanoparticles were washed once with methanol before they were finally collected with a magnet. To the BMEP-coated nanoparticles, another 0.3 mL of BMEP stock solution was added along with 0.7 mL chloroform to maintain the nanoparticle's stability during the polymerization reaction.

1.5 Polymer nanocomposite fabrication

The polymer nanocomposite was fabricated using the *in-situ* free-radical polymerization reaction of PMMA with some modification.[4] Briefly, 240 mg of methyl methacrylate (MMA) was added to the 10 mg BMEP-coated nanoparticles prepared in the previous step. The solution was mixed thoroughly via sonication. After that, 2.5 mg of azobisisobutyronitrile (AIBN) was added to the MMA/nanoparticle solution and sonicated until fully dissolved. The reaction vial was then partially sealed to allow the chloroform to evaporate during the polymerization reaction which was carried out at 70 °C for 2.5 hours. After that, the vial was placed under vacuum to evaporate any remaining solvent or unreacted MMA. Once fully dry, the weight of the polymer nanocomposite was measured, and the nanoparticle loading was determined by dividing the weight of added nanoparticles by the overall weight of the polymer composite.

The polymer nanocomposite was then dissolved in chloroform to form a viscous solution. Roughly 30-50 uL of the dissolved polymer nanocomposite was then taken out using a pipet and drop-casted on a clean glass slide substrate. The substrate was then placed under vacuum to evaporate the chloroform in a controlled manner and form a polymer nanocomposite thin film for the Faraday rotation measurements. The thickness of the polymer nanocomposite films was measured using a stylus profilometer as shown in the Table 1.

Table 1: Polymer nanocomposite film thicknesses

Polymer nanocomposite film	Thickness (μm)
PMMA-Fe_3O_4	90.0
PMMA-Fe_3O_4: 0.29% Tb^{3+}	25.7
PMMA-Fe_3O_4: 0.69% Tb^{3+}	26.6
PMMA-Fe_3O_4: 1.12% Tb^{3+}	35.5
PMMA-Fe_3O_4: 2.23% Tb^{3+}	37.6
PMMA-Fe_3O_4: 4.55% Tb^{3+}	24.9

2. Faraday rotation measurement

To reduce the effects of sample oxidation the samples were measured within two weeks of fabrication. The measurement apparatus can be seen in Figure 1, the setup is like what is seen in Pavlopoulos *et al.*[5] The light from a 980nnm pump driver diode is first linearly polarized and a beam sampler is used to pick off a small portion of the light to measure the intensity of the light. This creates a feedback loop with a PID laser servo controller allowing us to stabilize the laser power against polarization instability from the light delivery path. The light is then fed through a free space optical chopper to create a signal that can be detected using lock-in detection. A half waveplate on motorized rotation stage is used to bias the light to 45˚ as well as perform responsivity calibration. We focus the light through the sample and onto a mirror

with a long focal length lens (f=100mm). This double passes the MNP sample negating any residual polarization effects such as stress birefringence from the sample. The magnetic field is applied at DC using a simple homemade solenoid coil.

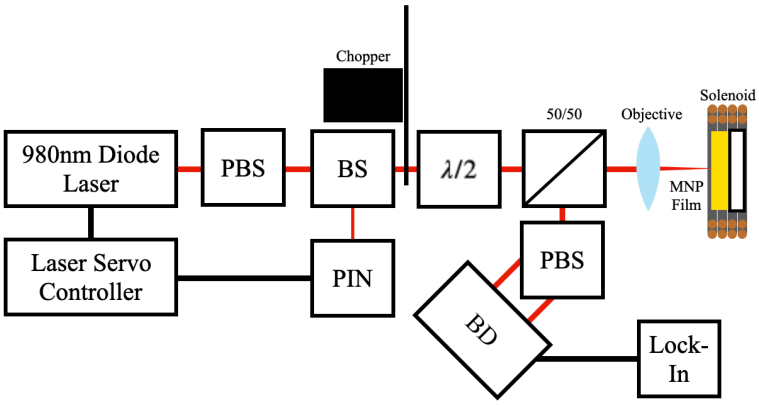

Figure S1: System schematic, PC: Polarization controller. ISO: Optical Isolator, PBS: Polarizing beam splitter, lam/2: Half waveplate, BS: beams sampler, PIN: Photodetector, BD: Balanced detector

The light returning from the sample is passed through a Wollaston prism polarization beam splitter onto an autobalanced detector (New Focus Nirvana 2017). The amplitude of the chopped optical signal is measured and recorded by a lock-in detector (SRS830). To perform an acquisition, the sample is mounted into the solenoid coil. The light first rotated by 0.6˚ (0.3˚ physical rotation of half waveplate) using the motorized mount. This serves to calibrate the responsivity of the system to the specific optical power incident on the detector (Nominally 300μW on each port). The solenoid coil is then energized at 3 different field strengths and the results averaged for 30 seconds.

We present a few final thoughts for the experimentalist. Firstly, measuring Faraday rotation using small mT DC fields can be challenging. Temperature fluctuations in both the bias waveplate and sample can cause the no applied field baseline to drift, which renders long integration periods inaccurate even with lock-in detection. This must be compensated for by thermally isolating the measurement apparatus or by performing measurements with AC magnetic fields as done in Pavlopoulos et al. work.[6]

3. Additional experimental results

3.1 Size optimization of nanoparticles

We performed a simple size sweep where the undoped nanoparticles were subjected to additional growth phases to increase the nanoparticle size. We found that the FOM was optimized at 15nm. The reduction in both the Verdet constant and FOM when larger particles were used is caused by the increased aggregation and scattering as these nanoparticles have strong magnetic interactions and tend to form clusters in solution as well as in the PMMA matrix. As a result, we opted for 15 nm for all Tb-doped

magnetite nanoparticles to achieve the maximum MO performance with the minimal impact from aggregation and scattering.

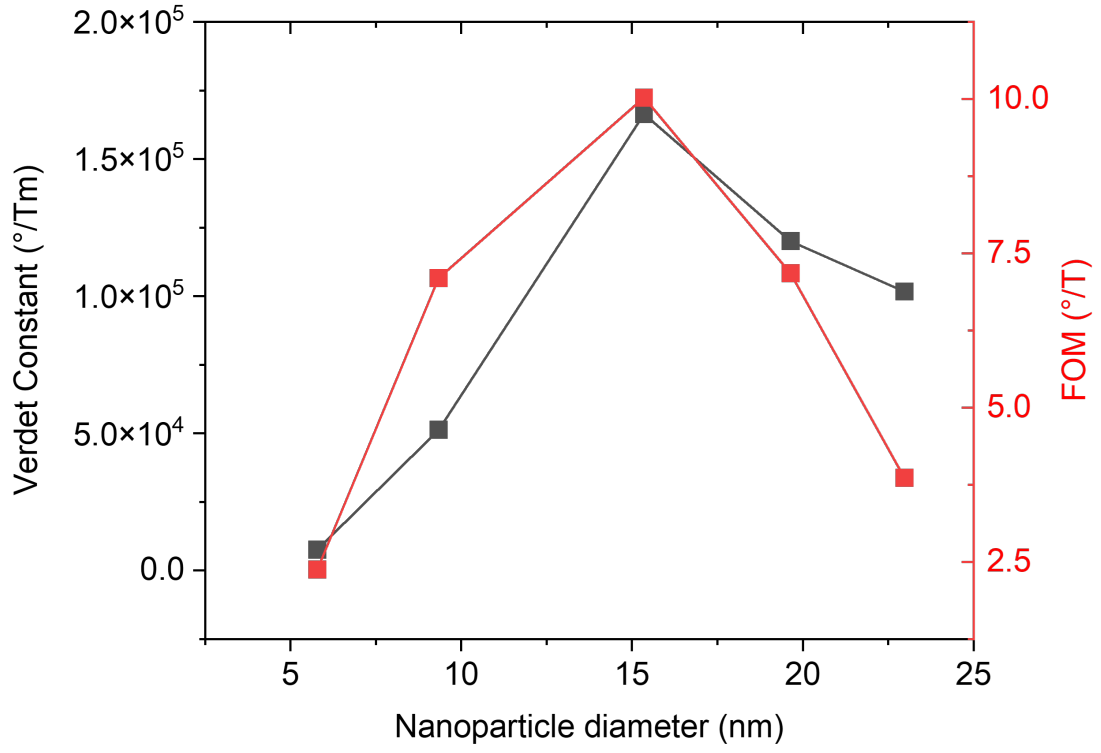

Figure S2: Verdet constant and FOM as a function of the magnetite nanoparticle size.

3.2 Structural analysis of pure and doped nanoparticles

We prepared fresh Fe_3O_4 and Fe_3O_4: Tb^{3+} (3) nanoparticles for X-ray diffraction (XRD), Raman spectroscopy, and photoluminescence (PL) spectroscopy. We chose these two samples since they represent our reference nanoparticles and the optimally doped nanoparticles in terms of Verdet constant and FOM as discussed in the main text. XRD spectra from 10 – 80 degrees two-theta (2.5 deg/min) were acquired on a SmartLab 9kW rotating anode diffractometer Rigaku (Rigaku Americas Corporation, Woodlands, TX, USA) utilizing Cu K-alpha radiation (1.54 Angstrom). K-beta radiation was removed with a Ni metal filter. The instrument was operating in Bragg-Brentano mode with the HyPix3000-SE detector set to 1D continuous acquisition. The beam profile was set to 5mm wide, and the axial divergence was reduced with symmetric 2.5-degree Soller slits on the incident and receiving optics path. Powder samples were loaded into a Si zero-background stage (MTI Corporation). All data was acquired and reduced using the Rigaku SmartLab Studio II software. The Raman spectra of the undoped and Tb-doped magnetite powders were collected using Renishaw InVia under 514 nm excitation. Lastly, the visible PL spectra of ethanol

dispersions of the undoped and Tb-doped nanoparticles were collected using Fluorolog-3 FL3-222 under 320 nm excitation.

As shown in Fig. S3 (A) below, both the undoped and doped samples show similar XRD peaks – closely matching the pure magnetite phase. The lattice parameters for the undoped nanoparticles are calculated to be 8.385 ± 0.008 Å while the Tb-doped magnetite nanoparticles have a lattice constant of 8.390 ± 0.009 Å. Previous work on Tb-doped magnetite nanoparticles reported only 0.25% increase in the lattice constant at a ~ 20% Tb^{3+} doping and no obvious changes in the XRD spectra for doped and undoped sample.[2] It is therefore not surprising that our lightly doped nanoparticles have an XRD spectrum that is indistinguishable from that of pure magnetite. Our calculated lattice constants are also in agreement with what has been reported for magnetite nanoparticles.[7] This XRD data presents strong evidence that the Tb^{3+} ions are incorporated in the magnetite lattice, possibly via substituting some of the Fe^{3+} ions as suggested by Rice et al.[2]

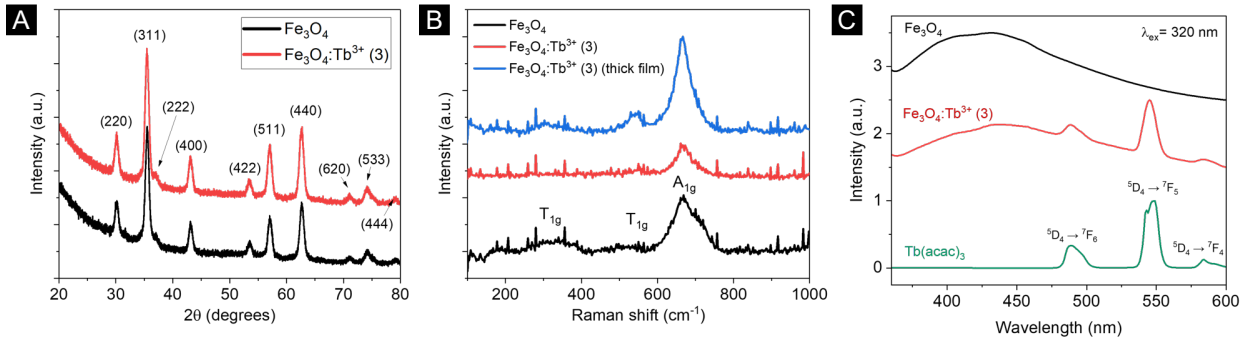

Figure S3: (A) XRD spectra of Fe_3O_4 and Fe_3O_4: Tb^{3+} (3) nanoparticles, (B) Raman spectra of the undoped and doped nanoparticles under 514 nm excitation, (C) PL spectra of the terbium precursor ($Tb(acac)_3$), Tb-doped magnetite, and pure magnetite.

The Raman spectra of the undoped and doped nanoparticles in Fig. S3 (B) show the main characteristic peaks of the magnetite phase: 670 cm^{-1} (A_{1g} mode), 550 cm^{-1} (T_{1g} mode), and 300 cm^{-1} (T_{1g} mode).[8] The relative peak intensities are also consistent with the typical spectrum of magnetite lattice in that the peaks associated with T_{1g} mode are weak compared to the strong A_{1g} mode. In the case of maghemite (Fe_2O_3) however, the Raman spectrum shows three strong peaks associated with the T_{2g}, E_g, and A_{1g} modes at 365, 511, and 700 cm^{-1} respectively.[8] The measured Raman spectra confirm that both Tb-doped and undoped nanoparticles are of the magnetite phase with no detectable shifts in the positions of the peaks.

Lastly, we investigated the photoluminescence spectra of the undoped and doped samples. The nanoparticles were dispersed in ethanol and added to quartz cuvettes to collect their visible emission (360 – 600 nm) under UV excitation (320 nm). For reference, we measured the emission of the Tb^{3+} precursor we use in the synthesis under similar conditions. As shown in Fig. S3 (C), the characteristic emission peaks

of the Tb^{3+} ions are present only in the Tb-doped nanoparticles, confirming their presence in the nanoparticles. The emission peaks at 480 nm, 545nm, and 585 nm corresponds to the Tb^{3+} transitions from the $^5D_4$ level to $^7F_6$, $^7F_5$, and $^7F_4$ levels respectively.[9]

4. References

(1) Sun, S.; Zeng, H. Size-Controlled Synthesis of Magnetite Nanoparticles. *J Am Chem Soc* **2002**, *124* (28), 8204–8205. https://doi.org/10.1021/ja026501x.

(2) Rice, K. P.; Russek, S. E.; Geiss, R. H.; Shaw, J. M.; Usselman, R. J.; Evarts, E. R.; Silva, T. J.; Nembach, H. T.; Arenholz, E.; Idzerda, Y. U. Temperature-Dependent Structure of Tb-Doped Magnetite Nanoparticles. *Appl Phys Lett* **2015**, *106* (6), 062409. https://doi.org/10.1063/1.4907332.

(3) Jin, Y.; Kishpaugh, D.; Liu, C.; Hajagos, T. J.; Chen, Q.; Li, L.; Chen, Y.; Pei, Q. Partial Ligand Exchange as a Critical Approach to the Synthesis of Transparent Ytterbium Fluoride–Polymer Nanocomposite Monoliths for Gamma Ray Scintillation. *J Mater Chem C Mater* **2016**, *4* (16), 3654–3660. https://doi.org/10.1039/C6TC00447D.

(4) Boyer, J. C.; Johnson, N. J. J.; Van Veggel, F. C. J. M. Upconverting Lanthanide-Doped NaYF4-PMMA Polymer Composites Prepared by in Situ Polymerization. *Chemistry of Materials* **2009**, *21* (10), 2010–2012. https://doi.org/10.1021/cm900756h.

(5) Carothers, K. J.; Lyons, N. P.; Pavlopoulos, N. G.; Kang, K.-S.; Kochenderfer, T. M.; Phan, A.; Holmen, L. N.; Jenkins, S. L.; Shim, I.-B.; Norwood, R. A.; Pyun, J. Polymer-Coated Magnetic Nanoparticles as Ultrahigh Verdet Constant Materials: Correlation of Nanoparticle Size with Magnetic and Magneto-Optical Properties. *Chemistry of Materials* **2021**, *33* (13), 5010–5020. https://doi.org/10.1021/acs.chemmater.1c00808.

(6) Pavlopoulos, N. G.; Kang, K. S.; Holmen, L. N.; Lyons, N. P.; Akhoundi, F.; Carothers, K. J.; Jenkins, S. L.; Lee, T.; Kochenderfer, T. M.; Phan, A.; Phan, D.; Mackay, M. E.; Shim, I. B.; Char, K.; Peyghambarian, N.; LaComb, L. J.; Norwood, R. A.; Pyun, J. Polymer and Magnetic Nanoparticle Composites with Tunable Magneto-Optical Activity: Role of Nanoparticle Dispersion for High Verdet Constant Materials. *J Mater0 Chem C Mater* **2020**, *8* (16), 5417–5425. https://doi.org/10.1039/D0TC00077A.

(7) Xu, Z.; Shen, C.; Hou, Y.; Gao, H.; Sun, S. Oleylamine as Both Reducing Agent and Stabilizer in a Facile Synthesis of Magnetite Nanoparticles. *Chemistry of Materials* **2009**, *21* (9), 1778–1780. https://doi.org/10.1021/CM802978Z

(8) Jubb, A. M.; Allen, H. C. Vibrational Spectroscopic Characterization of Hematite, Maghemite, and Magnetite Thin Films Produced by Vapor Deposition. *ACS Appl Mater Interfaces* **2010**, *2* (10), 2804–2812. https://doi.org/10.1021/AM1004943

(9) Kalusniak, S.; Castellano-Hernández, E.; Yalçinoğlu, H.; Tanaka, H.; Kränkel, C. Spectroscopic Properties of Tb3+ as an Ion for Visible Lasers. *Appl Phys B* **2022**, *128* (2), 1–16. https://doi.org/10.1007/S00340-022-07759-1